Cover effect in bedrock abrasion: A new derivation and its implications for the modeling of bedrock channel morphology

Jens M. Turowski, Dimitri Lague, Niels Hovius

Cover effect in bedrock abrasion: A new derivation and its implications for the modeling of bedrock channel morphology

Jens M. Turowski,[1,2] Dimitri Lague,[3,4] and Niels Hovius[1]

Received 21 September 2006; revised 2 July 2007; accepted 25 July 2007; published 3 November 2007.

[1] The sediment load of a bedrock river plays an important role in the fluvial incision process by providing tools for abrasion (the tools effect) and by covering and thereby protecting the bed (the cover effect). We derive a new formulation for the cover effect, in which the fraction of exposed bed area falls exponentially with increasing sediment flux or decreasing transport capacity, and explore its consequences for the model of bedrock abrasion by saltating bed load. Erosion rates predicted by the model are higher than those predicted by earlier models. In a closed system, the maximum erosion rate is predicted to occur when sediment supply is equal to transport capacity for a flat bed. By optimizing the channel geometry to minimize the potential energy of the stream and using representative values for both discharge and grain size, we derive equations for the geometry of a bedrock river and explore how predictions for width, slope, and bed cover vary as functions of drainage area, rock uplift rate, and rock strength. The equations predict a dependence of channel width on drainage area similar to the relations using a simple shear stress incision law. The slope-area relationship is predicted to be concave up in a log-log regime, with a curvature dependent on uplift rate. However, this curvature does not deviate sufficiently from a straight line to allow discrimination between models using empirical data. Dependence of channel width and slope on rock uplift rate can be separated into two domains: for low uplift rates, channel geometry is largely insensitive to uplift rate due to a threshold effect. At high uplift rates, there is a power law dependence. Bed cover is predicted to increase progressively downstream and to increase with increasing uplift rate. In our model, the width-to-depth ratio is a function of both tectonic and climatic forcing. This indicates that the scaling between channel width and bed slope is neither a unique indicator of tectonic forcing at steady state nor a signature of transience or steady state. We conclude that sediment effects need to be taken into account when modeling bedrock channel morphology.

Citation: Turowski, J. M., D. Lague, and N. Hovius (2007), Cover effect in bedrock abrasion: A new derivation and its implications for the modeling of bedrock channel morphology, *J. Geophys. Res.*, *112*, F04006, doi:10.1029/2006JF000697.

1. Introduction

[2] The erosion of nonglaciated landscapes is driven by fluvial incision into bedrock. Of several possible mechanisms, abrasion is often the dominant mode of fluvial incision [*Hartshorn et al.*, 2002; *Sklar and Dietrich*, 2004]. Abrasion is conceptually simple. A fraction of the kinetic energy of particles striking the bed may be expended on fracturing the rock and removing bed material. *Gilbert* [1877] was the first to realize that the amount of sediment transported by a river has two opposing effects on bedrock incision by abrasion: the erosion rate (1) increases with the number of particles available as tools for abrasion (the tools effect) and (2) decreases as sediment covers the bed and thereby protects the rock from erosion (the cover effect). Given the large amount of sediment carried by actively incising mountain rivers, it seems likely that the cover effect rather than the tools effect limits rates of erosion. The cover effect must be modeled adequately if the dynamics of bedrock rivers and the erosion processes within them are to be understood.

[3] *Moore* [1926] suggested that sediment supply could control whether a bedrock channel actively meanders through uplifted bedrock, and thereby have an effect on channel planform and cross-sectional geometry. *Shepherd* [1972] verified this concept for artificial channels in a series of experiments. More recently, several studies have addressed the influence of sediment flux on channel evolu-

[1]Department of Earth Sciences, University of Cambridge, Cambridge, UK.
[2]Now at Swiss Federal Institute for Forest, Snow and Landscape Research, Birmensdorf, Switzerland.
[3]Géociences Rennes, Université Rennes I, Rennes, France.
[4]UMR 6118, Institut National des Sciences de l'Univers, CNRS, Rennes, France.

0148-0227/07/2006JF000697

tion [e.g., *Wohl and Ikeda*, 1997; *Hancock and Anderson*, 2002; *Whipple and Tucker*, 2002; *Sklar and Dietrich*, 2006; *Wobus et al.*, 2006a, *Finnegan et al.*, 2007; *Turowski et al.*, 2007] and bedrock wear by experiment [e.g., *Sklar and Dietrich*, 2001; *Attal et al.*, 2006] and theoretical methods [*Foley*, 1980; *Kooi and Beaumont*, 1996; *Slingerland et al.*, 1997; *Sklar and Dietrich*, 1998, 2004]. Sediment supply effects and their influence on erosion models have been reviewed by *Sklar and Dietrich* [2006]. They stressed the fact that incision models without a cover term will overpredict incision rates for high sediment supply rates. These models also lack a fundamental coupling between the local channel dynamics (partly set by rock properties and uplift rate) and upstream sediment production and supply.

[4] Efforts to model the cover effect so far lack a physical basis and there is a mismatch between measurements of experimental erosion rates [*Sklar and Dietrich*, 2001] and theoretical predictions [*Sklar and Dietrich*, 1998, 2004], especially for high ratios of sediment supply to transport capacity. In nature, the problem is due in part to the difficulty of measuring bed load transport during flood events in mountain rivers. In addition, observed rapid changes of the degree of bed cover between floods hamper the meaningful definition of an incision model at geological timescales.

[5] In this paper, we build on the work by *Sklar and Dietrich* [1998, 2004, 2006] by deriving a new functional form for the cover effect based on a probabilistic argument. The model provides a physical explanation of the experimental results of *Sklar and Dietrich* [2001] on the relationship between erosion rate and sediment supply. We then use minimization of the river potential energy expenditure [*Lague et al.*, 2005a] to explore some consequences of our model for the geometry and bed cover of steady state bedrock rivers as a function of discharge, uplift rate and sediment supply.

2. Model Development and Justification

2.1. River Incision by Saltating Bed Load

[6] *Sklar and Dietrich* [1998, 2004] have developed a mechanistic model of river incision by abrasion of bedrock by saltating grains. In this model, the erosion rate is written as the product of three terms, describing (1) the volume of material removed at each particle impact V_i, (2) the rate of impact of particles per unit area I_r, and (3) the fraction of bedrock exposed to the flow R_a:

$$E = V_i I_r R_a. \tag{1}$$

For the terms V_i and I_r we use the expressions proposed by *Sklar and Dietrich* [2004], giving:

$$E = K S_e q_s R_a, \tag{2}$$

with

$$K = \frac{0.08 \Delta \rho g Y}{k_v \rho_w \sigma_t^2} \left[\frac{\tau^*}{\tau_c^*} - 1 \right]^{-1/2} \tag{3}$$

and

$$S_e = \left[1 - \left(\frac{u^*}{w_f} \right)^2 \right]^{3/2}. \tag{4}$$

Here g is the gravitational acceleration at the Earth's surface, Y Young's modulus of the substrate, k_v a dimensionless rock resistance coefficient, σ_t the rock tensile strength, $\Delta\rho = \rho_s - \rho_w$ where ρ_w and ρ_s are the densities of water and sediment respectively, $\tau^* = \tau_b / \Delta \rho g d$ the Shields stress and τ_c^* the critical Shields stress for the onset of motion of sediment, where τ_b is the bed shear stress and d the sediment grain diameter. w_f is the particle fall velocity in still water, $u^* = (\tau_b/\rho_w)^{1/2}$ the shear velocity, and q_s is the sediment flux per unit width in the river. All definitions are listed at the end of the paper. K is a measure of the substrate erodibility, and also incorporates sediment motion dynamics. The suspension effect term S_e accounts for the increasing proportion of mobile sediment carried in suspension with rising shear stress. It can be neglected for small values of the transport stage $T_s = \tau^*/\tau_c^* \leq 10$, corresponding to shear stresses below the threshold for suspension [*Sklar and Dietrich*, 2004], giving

$$E = K q_s R_a. \tag{5}$$

This approximation applies in all calculations done in this paper, except when stated otherwise.

2.2. Cover Effect

2.2.1. Derivation in the Context of Abrasion Experiments

[7] Previous functional expressions for the cover effect have been linear models rooted in the balance of sediment supply and sediment transport capacity [*Slingerland et al.*, 1997; *Sklar and Dietrich*, 1998, 2004] but lacking a physical basis. Bedrock erosion by particle impact has been investigated in experiments using circular or recirculating flumes [*Sklar and Dietrich*, 2001; *Attal et al.*, 2006]. These experiments are closed systems, in which a fixed amount of sediment m_s is introduced. When steady flow conditions are reached, the flow capacity defines the maximum mass m_t that can be transported as bed load. In our approach we assume that the transport capacity is uniform throughout the considered area and independent of the amount of sediment in the flow. If $m_s > m_t$, then part of the sediment is not transported and remains immobile on the bed, shielding the bed from abrasion. This is a static cover effect. When $m_s < m_t$, all sediment is mobile, but a shielding effect is still expected: with increasing m_s, the concentration of saltating particles near the bed increases to the point where a significant number of near-bed grain-grain collisions occurs, and the number of grain-bed collisions is reduced. This is a dynamic cover effect. Furthermore we assume that once sufficient cover is present, erosion rate does not vary with the thickness of sediment at a point.

[8] The channel bed erosion rate is proportional to the fraction of bed area $R_a = a_{\exp}/a_{tot}$ exposed to the flow (equation (3)) [*Sklar and Dietrich*, 1998, 2004]. Here $a_{\exp}$ is the area exposed to impacting particles and a_{tot} is the total bed area. Let m be the ratio $m = m_s/m_t$. For $m_s > m_t$, when m is increased by a small amount dm, a fraction $a_{\exp}/a_{tot}$ of this amount will fall on exposed bedrock and cover it, while the remainder falls on parts of the channel bed that are already (statically) covered by sediment. Hence

$$dR_a = -R_a dm. \tag{6}$$

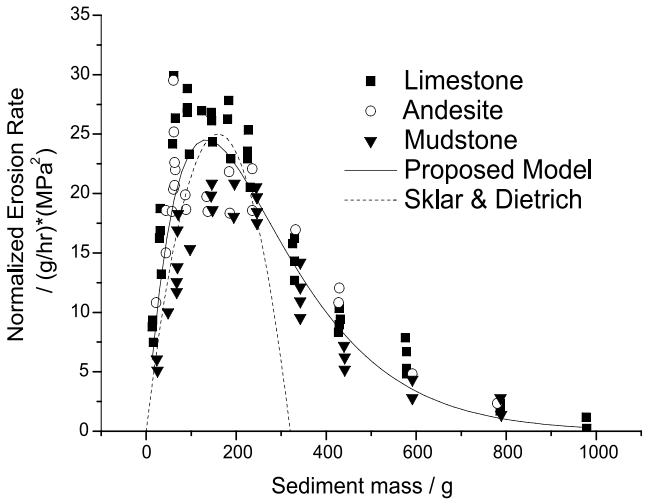

Figure 1. Erosion rates as function of sediment load measured by *Sklar and Dietrich* [2001] with an erosion mill. The erosion rate is normalized to collapse all data onto the same curve. The solid line shows the best fit using equation (10), and the dashed line shows a fit using the linear model for the cover effect by *Sklar and Dietrich* [1998, 2004].

The minus sign occurs because the fraction of exposed area decreases when sediment is added. Equation (6) also applies when $m_s < m_t$: for any increase in m_s, part of the added sediment will fall on previously bare bed and thus contributes to a reduction of R_a. The remainder falls on previously (dynamically) covered bed areas. Equation (6) assumes that it is equally likely for sediment to impact or fall on any part of the bed. It could well be the case that variations in local flow conditions or bed roughness, for example between areas with and without cover, affect the likelihood of sediment falling at a particular site. To reflect a difference in the probability of impact or accumulation on a unit bed area between exposed and covered areas, a factor φ is introduced:

$$dR_a = -\varphi R_a dm. \tag{7}$$

It is reasonable to assume that the value of φ depends on the precise geometry of the bed, and possibly on flow conditions, and that $\varphi \neq 1$. φ is less than one when it is more probable for sediment to fall on statically or dynamically covered areas, and greater than one when it is more probable for sediment to fall on uncovered areas. Cross-channel variations of sediment supply or transport capacity can, in principle, be modeled by appropriately choosing φ. In the absence of direct constraints, $\varphi = 1$ will be used in further calculations.

[9] Integrating equation (7):

$$R_a = \frac{a_{\exp}}{a_{tot}} = \kappa e^{-\varphi m} = e^{-\varphi m}, \tag{8}$$

where κ is an integrative constant which can be fixed to one by stipulating that $R_a = 1$ at $m_s = 0$. Equation (8) shows that the bed surface dynamically or statically exposed to abrasion decreases exponentially with increasing sediment supply. Substituting equation (8) into equation (5) and working with m_s instead of q_s, we obtain an expression for fluvial bedrock erosion including the effect of bed cover:

$$E = K_m m_s e^{-\varphi \frac{m_s}{m_t}}, \tag{9}$$

where K_m has a similar function as K.

[10] Figure 1 shows data obtained by *Sklar and Dietrich* [2001] in experiments investigating the dependency of erosion rate on sediment load. The erosion rate has been normalized with respect to tensile strength of the bedrock, sediment density, and bed area to collapse data for several lithologies onto a single curve. In the transformed coordinates, the equation is written as

$$E' = K' m_s e^{-\varphi \frac{m_s}{m_t}}. \tag{10}$$

Here E' is the normalized erosion rate and K' the corresponding erodibility factor. Details of the transformation between K and K' can be found in Appendix A.

[11] In Figure 1 the erosion rate rises to a maximum and then falls off, rapidly at first and then approaching zero asymptotically, as the sediment load is increased. Where the tools effect dominates, an increase of the sediment load leads to higher erosion rates. Beyond the erosion maximum, where the cover effect dominates, an increase of sediment load leads to greater bed cover and decreased erosion rates. The solid line represents the best fit by nonlinear regression using equation (10) with $K' = (0.50 \pm 0.02)$ MPa^2 h^{-1} and $\varphi/m_t = (7.5 \pm 0.2) \times 10^{-3}$ g^{-1}. Assuming that in a closed system $m_s/m_t = q_s/q_t$ (see section 2.2.2), we find that equation (10) yields a better fit to the data than the parabolic model of *Sklar and Dietrich* [1998, 2004] (dashed line in Figure 1). Note that in the *Sklar and Dietrich* [1998, 2004] cover model, $R_a = 1 - m$ is a Taylor expansion to first order of equation (8), using $\varphi = 1$. As such, it provides a good fit to the data where the tools effect dominates (left of maximum in Figure 1), but the functions diverge for larger sediment loads, where the cover effect dominates. The exponential model derived above fits the experimental data well in both domains.

2.2.2. Application to Natural Channels

[12] A section of a natural channel is an open system in which bed load is continuously supplied from upstream and exported downstream, with the possibility of local deposition. In the channel section, the rate of change of the thickness h of sediment stored is a function of the gradient of unit sediment flux q_f along the stream:

$$\frac{dh}{dt} = E + F - \frac{dq_f}{dx}, \tag{11}$$

where x is the distance along the stream, and F is the net transfer from suspended load to bed load [cf. *Paola and Voller*, 2005]. Hence resolution of the extent of bed cover at any time $t + dt$ requires knowledge of the amount of sediment m_i stored in the channel at t, the bed load sediment supply q_s and the local bed load transport capacity q_t. Two scenarios can occur. (1) When $m_i = 0$ or when the system can transport all the sediment supplied and locally stored,

resulting in unit sediment flux q_f, then $m_s/m_t = q_f/q_t$, and the cover is defined by equation (8) as

$$R_a = e^{-\varphi\frac{q_f}{q_t}}. \quad (12)$$

(2) When $m_i \geq 0$ and the system is over capacity, then $m_s/m_t = q_s/q_t$, and equation (6) gives the variation of R_a as a function of the existing cover related to m_i, R_a(t):

$$dR_a(t+dt) = -R_a(t)d\frac{q_s(t+dt)}{q_t(t+dt)}. \quad (13)$$

Equation (13) indicates that the cover at any time depends on the history of the ratio of sediment supply to sediment transport capacity. Thus, when some sediment is stored in the channel, no unique relationship exists between the cover extent (dynamically and statically) and the ratio q_s/q_t. Prediction of the transient dynamics of cover and channel geometry would require a 1D or 2D numerical model [e.g., *Hancock and Anderson*, 2002] with coupled hillslopes and channel. This is beyond the scope of this paper. Instead, we have focused our analysis on the sensitivity of erosion rates to dynamic cover effects (equation (12) with $q_f = q_s$), and prediction of the steady state geometry and bed cover of bedrock river channels.

2.2.3. Rivers in Steady State

[13] At steady state, channel geometry (width, slope) and bed cover are constant on average over timescales significantly longer than the duration of a flood. For a steady bed cover to be attained, q_t must be larger than q_s, or sediment would fall out and bed cover would increase with time toward the state $R_a = 1$.

[14] When $q_s < q_t$ at steady state, there is no permanent, static cover (excess capacity would remobilize it). Then, only dynamic cover may shield the bed. In this case, combining equation (12) with $q_f = q_s$, and equation (5) gives the erosion law

$$E = Kq_s e^{-\varphi\frac{q_s}{q_t}}. \quad (14)$$

When $q_s = q_t$, there can be a permanent static cover. Its extent is a function of the sediment transport history and cannot be predicted a priori with a model such as equation (14). This static cover is constant in time when the sediment supplied to the channel reach equals the sediment exported from the reach. Estimation of the static cover extent requires explicit tracking of the amount of sediment stored in a channel reach prior to attainment of steady state. We have not modeled these effects, and focused instead on systems with a dynamic cover.

2.3. Relating the Equation to Bed Geometry

[15] To allow comparison with erosion rates in natural rivers, equation (12) must be written in terms of observable parameters. By using equations for the bed shear stress, the channel geometry, the flow resistance, and the bed load transport capacity, the erosion rate can be expressed as a function of channel bed slope and hydraulic radius. Bed shear stress is given by

$$\tau_b = \rho_w g R_h S. \quad (15)$$

The Manning flow resistance equation

$$V = \frac{1}{n}R_h^{2/3}S^{1/2} \quad (16)$$

can be used to calculate the mean flow velocity [*Manning*, 1891]. Here V is the flow velocity averaged over the channel cross section, n the Manning friction coefficient, R_h the hydraulic radius of the channel and S the energy slope, approximated by the channel bed slope. Assuming a rectangular channel cross section, the hydraulic radius can be written as

$$R_h = \frac{DW}{2D+W} = \left(\frac{nQ}{DWS^{1/2}}\right)^{3/2}. \quad (17)$$

Here W and D are the flow width and depth, respectively, and Q is the water discharge. Flow velocity V is related to W, D and Q by the continuity equation $Q = VWD$.

[16] For compatibility, we follow *Sklar and Dietrich* [2004] in using the *Fernandez Luque and van Beek* [1976] bed load equation to calculate the unit transport capacity

$$q_t = 5.7\rho_s\left(\frac{\Delta\rho g d^3}{\rho_w}\right)^{1/2}(\tau^* - \tau_c^*)^{3/2}, \quad (18)$$

where d is the median grain size. Substituting expressions (15) and (18) into (14) gives

$$E = Kq_s \exp\left\{-\frac{\varphi q_s}{5.7\rho_s}\left(\frac{\rho_w}{\Delta\rho g d^3}\right)^{1/2}\left(\frac{\rho_w R_h S}{\Delta\rho d} - \tau_c^*\right)^{-3/2}\right\}, \quad (19)$$

with

$$K = \frac{0.08\Delta\rho g Y}{k_v\rho_w\sigma_t^2}\left[\frac{\rho_w R_h S}{\tau_c^*\Delta\rho d} - 1\right]^{-1/2}. \quad (20)$$

Equation (19) casts fluvial bedrock erosion in terms of variables that can be measured on natural systems. In the following section, we explore the sensitivity of model erosion rates to parameters in equations (19) and (20), and compare our results with the *Sklar and Dietrich model* [2004].

3. Controls on Erosion Rates and Comparison to the Linear Model

[17] Equation (19) combines a mechanistic model for abrasion with an exponential model for the cover effect. Inserting parameter values from sites at South Fork Eel Creek (SFEC), Mendocino County, California, USA [*Sklar and Dietrich*, 2004] and Lushui Station, Liwu River (LW), Taiwan [*Hartshorn et al.*, 2002] into this expression, we have estimated erosion rates for a range of conditions in natural channels. For comparison, we have made matching calculations using *Sklar and Dietrich*'s [2004] original model, with a linear expression for the cover effect. Parameter values at the reference sites are listed in Table 1. A value for $k_v \sim 10^6$ has been estimated from the data in

Table 1. Parameter Values for South Fork Eel Creek, Mendocino County, California, United States, and Lushui, Liwu River, Taiwan[a]

Input Parameter	South Fork Eel Creek	Lushui
Channel slope S	0.0053	0.02
Discharge Q, $m^3\ s^{-1}$	39.1	59.4
Median grain diameter d, m	0.060	0.042
Unit sediment supply q_s, kg $m^{-1}\ s^{-1}$	2.37	7.17[b]
Channel width W, m	18.0	36.7[b]
Channel depth D, m	1.2[b]	0.7[b]
Hydraulic radius R_h, m	1.06[b]	0.57[b]
Roughness n	0.035	0.035
Rock tensile strength σ_t, MPa	7.0	9.5
Rock elastic modulus Y, MPa	5.0×10^4	5.0×10^{4b}
Rock resistance parameter k_v	10^{6b}	10^{6b}
Critical Shield's stress τ_c*	0.03	0.07
Sediment density ρ_s, kg m^{-3}	2650	2650
Water density ρ_w, kg m^{-3}	1000	1000
Instantaneous erosion rate, mm a^{-1}	20[b]	31[b]
Yearly averaged erosion rate, mm a^{-1}	0.9[b]	16[b]
Drainage area, km^2	112[2]	435

[a]South Fork Eel Creek [*Sklar and Dietrich*, 2004] and Lushui [*Hartshorn et al.*, 2002].
[b]Calculated/estimated in this study.

Figure 1 (details are given in Appendix A). The value of the bed cover factor φ was set equal to one. For SFEC we have assumed a rectangular cross section in accordance with our statements in section 2.3. The channel cross section at LW has been taken from a detailed survey [*Hartshorn et al.*, 2002]. Representative discharge, sediment supply, and instantaneous erosion rate have been calculated using the method of *Sklar and Dietrich* [2006]. This method partitions the flow distribution into an erosive high flow and a nonerosive low flow. All sediment is assumed to be transported at high flow. Only then is bedrock incised. To calculate yearly average erosion rates, instantaneous erosion rates during high flow have been multiplied by the fraction of time over which high-flow conditions prevail.

[18] Figure 2 shows model erosion rates as a function of sediment flux using the linear model (dashed line) and the exponential model (solid line) for the cover effect, for the reference sites in SFEC (Figures 2a and 2b) and the LW (Figures 2c and 2d). Predictions by the two models differ in two important ways. First, maximum erosion rates predicted by the model with an exponential cover effect are ~1/3 higher than those predicted by the model with a linear cover effect. Secondly, the linear model predicts zero erosion for

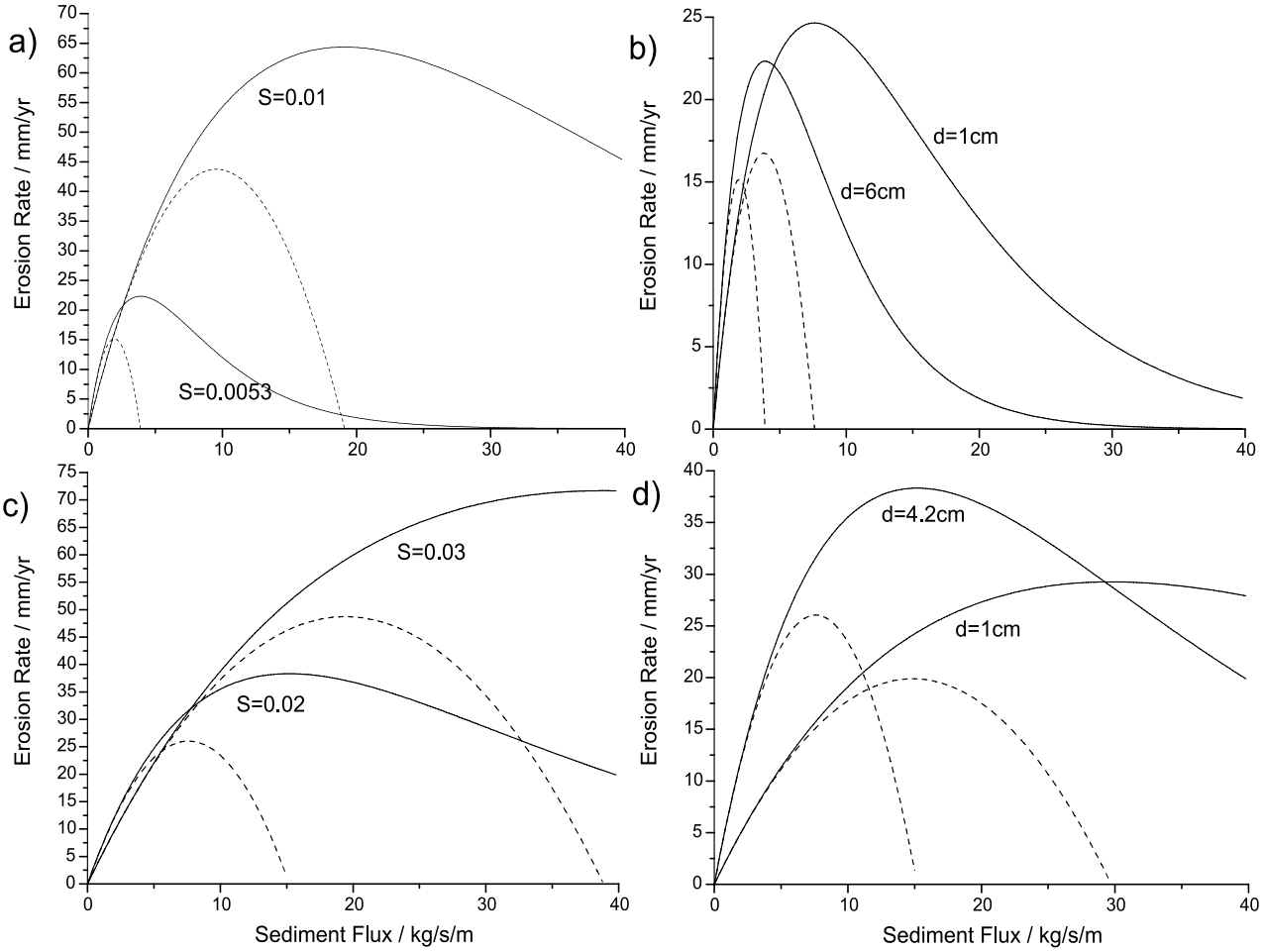

Figure 2. Comparison of the predictions of the abrasion model by saltating bed load [*Sklar and Dietrich*, 1998, 2004] using the linear (dashed lines) and the exponential (solid line) model for the cover effect. Predictions are shown for (a and b) South Fork Eel Creek and for (c and d) Lushui. S gives the value of channel bed slope, and d gives the value for median grain size used in the calculation.

values of sediment flux above the transport capacity. In contrast, the exponential model predicts erosion rates to peak at $q_s = q_t/\varphi$, i.e., when the sediment flux is equal to the transport capacity, assuming $\varphi = 1$. Beyond this point erosion rates decay with increasing sediment flux, approaching zero asymptotically. Erosion rates predicted with the exponential model are higher than for the linear model and the difference increases with increasing sediment supply.

[19] Figures 2a and 2c compare predictions for two different values of channel bed slope. Slope is the main control on the energy available in the flow and hence on erosion rates. Increasing the slope leads to increased erosion rates over most of the range of sediment flux values, especially for large fluxes. By comparison, grain size is a lesser control on erosion rates (Figures 2b and 2d). A decrease of the median grain size may lead to an increase (Figure 2b) or a decrease (Figure 2d) in the maximum erosion rate and to a shift in the position of the maximum to a higher sediment flux value.

4. Channel Geometry at Steady State

[20] The erosion law derived above (equation (19)) can be used to predict bedrock channel width, slope and bed cover at steady state, and their dependence on discharge, sediment supply, and incision rate. We compare these predictions to natural channel geometries and previously published models. As discussed in section 2.2.2, these predictions are only valid for the region $q_s < q_t$.

[21] Equation (19) has two unknowns (W and S). It is therefore impossible to independently define the slope and the width of a river at steady state for a given set of boundary conditions [*Lague et al.*, 2005a]. Often this problem has been solved by imposing an empirical relation [e.g., *Lague et al.*, 2005b; *Whipple and Tucker*, 1999]. In that approach, width cannot vary with incision rate, although it has been found to do so in nature and experiment [*Duvall et al.*, 2004; *Finnegan et al.*, 2005; *Harbor*, 1998; *Lavé and Avouac*, 2001; *Turowski et al.*, 2006; *Amos and Burbank*, 2007; *Whittaker et al.*, 2007], and numerical models [*Stark*, 2006; *Wobus et al.*, 2006b]. In contrast, minimizing the potential energy expenditure of the river by minimizing the slope for a given incision rate, and using a simple shear stress incision law, leads to predictions for the scaling of width, slope and discharge, and qualitatively good predictions for the dependence of channel geometry on incision rate and rock erodibility [*Lague et al.*, 2005a]. Such extremal hypotheses are a common approach in regime theory when treating alluvial river systems [e.g., *Huang and Nanson*, 2002; *Eaton et al.*, 2004; *Huang et al.*, 2004]. If the channel is in an energy configuration higher than the minimum, excess energy is expended to change channel shape. We use this approach here, but with the new erosion law (equation (19)). A complete discussion of underlying assumptions and their justification will be offered elsewhere. The full derivation of the steady state equations is given in Appendix B. Because of the complexity of this treatment (equation (B17)) and the large number of variables it involves, we present only one worked-out case to illustrate the general functional form of relations between steady state channel morphology and boundary conditions. For our calculations we use an average precipitation rate $P = 2$ m a^{-1}, a critical Shields stress $\tau_c^* = 0.03$, $B = 0.1$ m kg^{-1} s (equation (B8)), $C = 2.5 \times 10^4$ m^{-2} (equation (B9)), and $n = 0.035$ m$^{-1/3}$ s, close to conditions in the Liwu River.

[22] Using steady state relations for landscape evolution

$$Q = PA \tag{21}$$

$$Q_s = \beta UA \tag{22}$$

$$E = U, \tag{23}$$

steady state bedrock channel width and slope can be derived as functions of the upstream drainage area A, the average precipitation rate P, and the rock uplift rate or base level lowering rate U. The fraction of sediment transported as bed load β is assumed to be equal to 0.4 in the following.

4.1. Scaling With Drainage Area

[23] Figure 3 is a numerical summary of the dependence of channel slope and width on drainage area, for various uplift rates. The channel bed slope shows a concave-up profile in log-log space, the curvature of which is more pronounced for higher uplift rates. The proportion of alluvial cover steadily increases with drainage area (Figure 3c). This behavior contributes to a greater curvature of the slope area relationship in comparison to a shear stress erosion model without tools and cover effect: for small drainage areas (i.e., sediment flux), the channel must steepen when the drainage area is reduced, to compensate for the relatively low number of tool impacts per unit area of channel bed (tool-starved regime); for large drainage areas, the slope decreases less rapidly than with the simple shear stress model when drainage area is reduced, because a high enough sediment transport capacity must be maintained to allow for erosion of bedrock. Our model predicts a progressive downstream transition from a tools- to a cover-dominated regime, corresponding to a progressive alluviation of the bedrock channel. This is broadly consistent with field observations [e.g., *Snyder et al.*, 2003a].

[24] Next, we consider the channel width-area scaling predicted by the model. For large drainage areas, the predicted scaling converges with the observed power law scaling in bedrock rivers with a power of $\sim$0.5 [*Whipple*, 2004] (Figure 3); the point of convergence shifts to larger drainage areas with increasing uplift rate. For example, for $U = 0.5$ mm a^{-1}, a power law is a good approximation for drainage areas larger than $\sim$5 km^2; for $U = 1.0$ mm a^{-1} the critical drainage area increases to $\sim$10 km^2. For drainage areas smaller than this cutoff value, the gradient of the curve in log-log space is larger than 0.5, implying that in these small catchments, channel width decreases more rapidly with decreasing drainage area. This effect offsets the scarceness of tools in channels with small drainage areas, and secures a sufficient rate of particle impacts on the channel bed to counter the imposed rock uplift.

[25] The width-to-depth ratio increases with increasing drainage area (Figure 3d). The precise shape of the curve and the total increase over the tested range of drainage areas

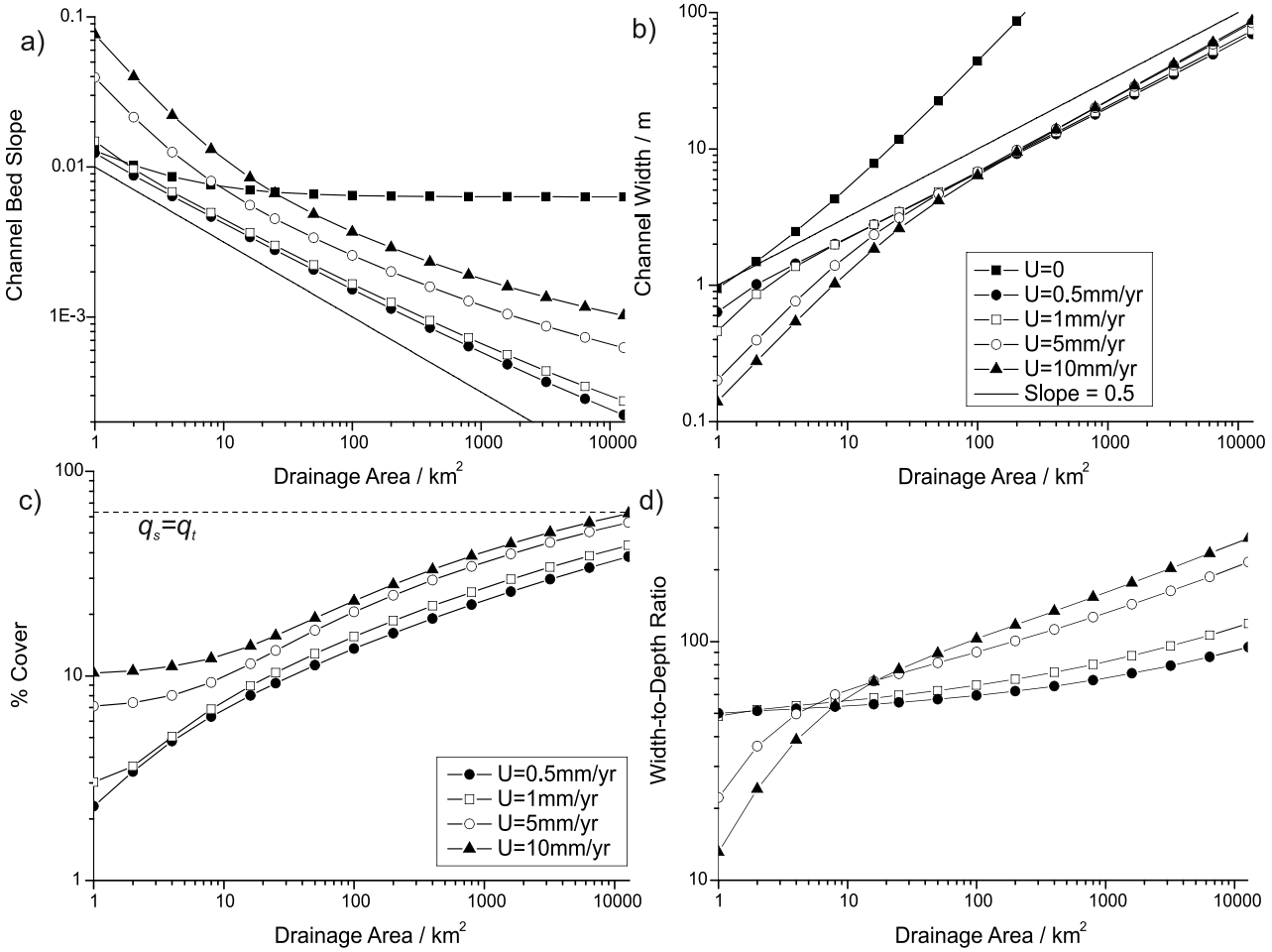

Figure 3. (a) Slope, (b) width, (c) bed cover dependence on drainage area, and (d) dependence on drainage area. The solid line is a power law with a power of −0.5 on the slope plot and 0.5 on the width plot. In Figure 3c, the dashed line marks the transition between detachment-limited and transport-limited conditions.

varies slightly with uplift rate. For small drainage areas (<10 km^2), an increase in uplift rate results in a decrease of the width-to-depth ratio, and for larger drainage areas an increase in uplift rate results in an increase of the width-to-depth ratio. This reversal is related to the slower increase in bed cover at low-drainage areas (Figure 3c).

[26] A further point of interest is the predicted linear scaling of both width and slope with drainage area for $U = 0$. The predicted behavior is due to equation (22), which only allows solutions with $Q_s = 0$ for $U = 0$. This is not a realistic situation and the model must be extended to describe sediment transport explicitly for this boundary condition.

4.2. Scaling With Uplift Rate and Sediment Supply

[27] The dependence of slope and width with rock uplift rate is shown in Figure 4. The graphs in Figure 4 extend to unnaturally high uplift rates of 10 m a^{-1} to show the full behavior of the curve. For conditions different from the ones used here, the curves may shift to the left, to lower uplift rates. For all drainage areas, channel slope is more sensitive than channel width to uplift rate (see also Figure 3), but two regimes are observed. At small uplift rates ($U < 1$ mm a^{-1}) the channel geometry is almost insensitive to variations in uplift rate. At higher uplift rates, slope increases rapidly according to a power law with an exponent of ~1.45, and width decreases more slowly according to a power law with an exponent of ~−0.45. The complex form of equations (B12)–(B17) makes a direct interpretation of these results difficult, but a comparison with predictions using a simple linear shear stress incision law of the form [*Howard and Kerby*, 1983; *Howard*, 1994; *Whipple and Tucker*, 1999]

$$E = k_e(\tau_b - \tau_c) \tag{24}$$

instead of equation (13) gives some insights. Using the optimization of potential energy expenditure and equation (24), *Lague et al.* [2005a] found the following steady state solutions:

$$W = 2^{8/13} n^{6/13} \left[\frac{\tau_c}{\rho_w g} + \frac{U}{\rho_w g k_e}\right]^{-3/13} (PA)^{6/13} \tag{25}$$

$$S = \left(\frac{8}{n}\right)^{6/13} \left[\frac{\tau_c}{\rho_w g} + \frac{U}{\rho_w g k_e}\right]^{16/13} (PA)^{-6/13}. \tag{26}$$

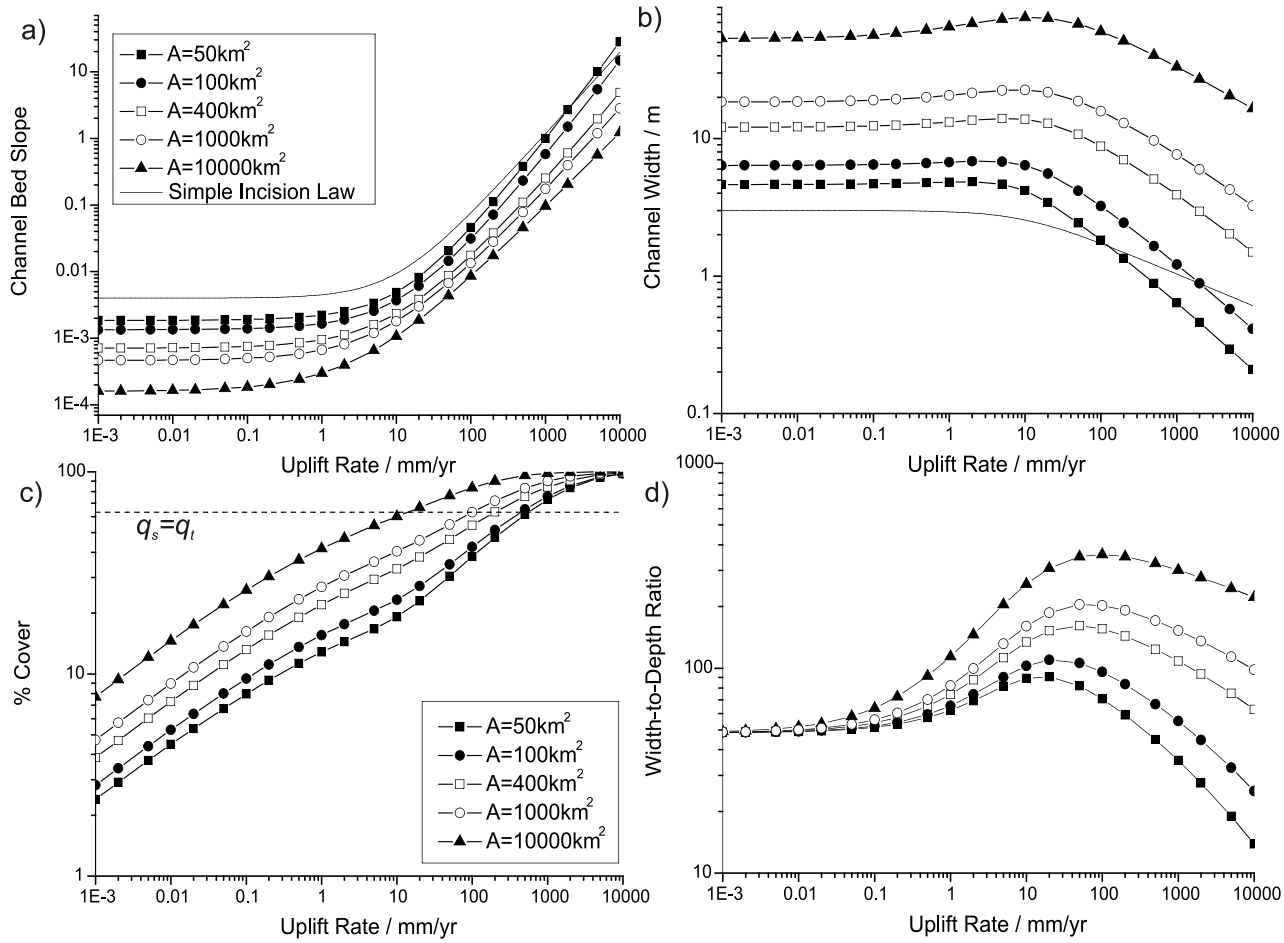

Figure 4. (a) Slope, (b) width, (c) bed cover dependence on uplift rate, and (d) dependence on uplift rate. The solid line in Figures 4a and 4b gives prediction using a simple incision law (equations (25) and (26)). In Figure 4c, the dashed line marks the transition between detachment-limited and transport-limited conditions.

These solutions are shown as solid lines in Figure 4. To first order, the evolution of the channel bed slope with uplift rate is similar for both incision laws, suggesting that stream long-profile response to uplift rate can be adequately modeled by equation (24), at least for drainage areas smaller than 10,000 km^2, and sediment flux effects do not need to be taken into account. This may partly explain the success of the stream power erosion law, as most studies focus on long-profile development. The insensitive region for low uplift rates corresponds to the case where

$$\frac{\tau_c}{\rho_w g} > \frac{U}{\rho_w g k_e}, \tag{27}$$

and the uplift term can be neglected. In this domain channel response is threshold limited and the channel geometry is set by the critical shear stress and the water discharge, similar to what has been described for incising gravel bed rivers [*Talling*, 2000]. For large U, the threshold term can be neglected and channel response is dominated by uplift. The slope uplift rate relationship follows a power law whose exponent is essentially a function of the friction law used (16/13 for the Manning friction law [*Lague et al.*, 2005a]). In the sediment supply-dependent model this exponent varies slightly with drainage area, a sensitivity that is not found in the simple shear stress model (equation (26)).

[28] Channel width-uplift rate relations for the two incision laws are different. Although threshold-limited and uplift-limited regimes are predicted for low and high uplift rates, respectively, the width-uplift relation for the simple shear stress model does not show a central maximum and has a much lower gradient at high uplift rates than that obtained with a sediment-supply dependent incision law including a tools and cover effect. The maximum in the width-uplift relation for our incision law corresponds to a decrease in the rate of increase of the cover extent (Figure 4c). A similar functional form, but more pronounced, can be seen in the relationship between width-to-depth ratio and uplift rate (Figure 4d). In our model, increasing uplift rate results in an increase of the sediment supply. Equation (17) stipulates that the erosion rate increases because of increased sediment flux, and in order to maintain a match with the imposed uplift rate, channel width and slope must adjust. As the uplift rate increases above the threshold-limited regime, erosion rates increase approximately linearly with sediment supply (and hence uplift rate) and the channel is predicted to

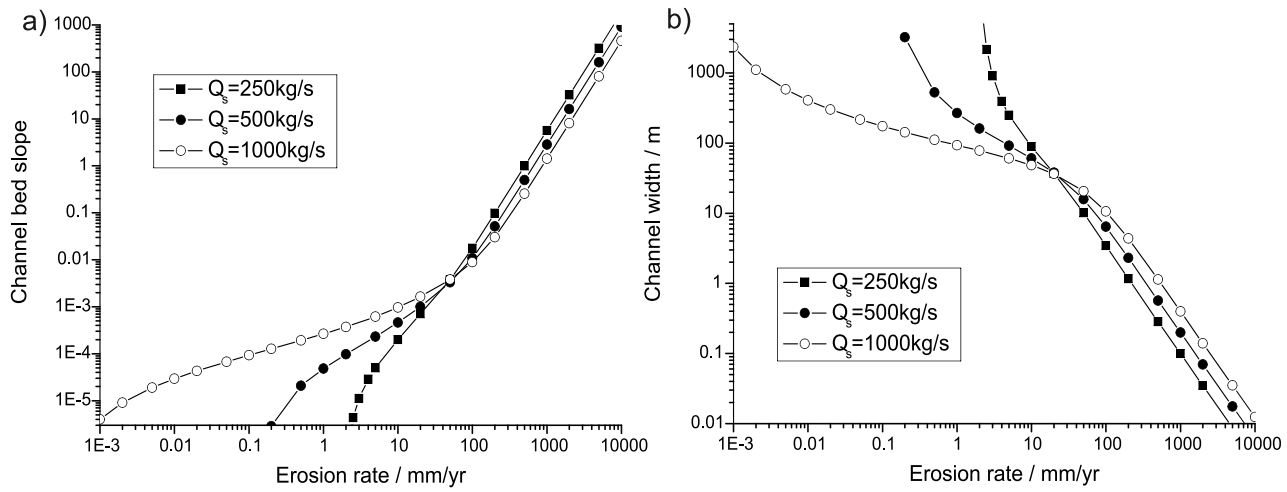

Figure 5. Slope and width as functions of erosion rate; sediment supply is held constant. $Q = 60\ m^3\ s^{-1}$.

widen in response. For large uplift rates, erosion rates increase slowly with sediment supply, and the channel width is reduced to focus erosion.

[29] Figure 5 shows solutions for channel width and slope as functions of erosion rate E, with constant discharge Q and sediment supply Q_s. The parameterization corresponds to a river with very large sediment discharge crossing a localized zone of rapid rock uplift that does not contribute sediment to the channel. At high erosion rates both the width-erosion and slope-erosion relationships approximate a power law whose exponent is independent of sediment discharge. At lower erosion rates, $E < 10$ mm a^{-1} in the example, the sensitivity of channel slope and width to erosion rate increases with decreasing sediment flux. Channels with a small sediment supply are starved of tools for incision, and are expected to contract in order to maintain a sediment flux per unit channel width required to meet the imposed erosion rate.

4.3. Scaling With Erodibility

[30] Finally, we consider the effects of variations of substrate erodibility on channel geometry and bed cover (Figure 6), using the ratio of Young's modulus to the square of the rock tensile strength (cf. equation (3)) as a proxy for erodibility similar to k_e (cf. equations (25) and (26)). The range of values for this ratio in Figure 6 covers all common rock types. Typical values are 5×10^{-4} Pa^{-1} for basalts, 10^{-3} Pa^{-1} for marble, and 10^{-2} Pa^{-1} for sandstones and shales; that is, rock strength decreases for increasing ratio. The values used for LW and SFEC are 5.5×10^{-4} Pa^{-1} and 10^{-3} Pa^{-1}, respectively. Channel geometry becomes less sensitive to rock strength as drainage area increases, and strong dependencies are only predicted for very hard rocks such as andesites and basalts, assuming that discontinuities in the rock mass do not dominate fluvial erosion. Slope, width, and width-to-depth ratio are independent of rock strength for ratios greater $\sim 2 \times 10^{-3}$ Pa^{-1}. This is due to a threshold effect (cf. equations (25) and (26) and the discussion on control of rock uplift rate in section 4.2). For weak substrates, low channel slope and large width combine to give a shear stress just above the threshold, and erosion rates can only be adjusted by varying the extent of bed cover. Channel slope increases when the ratio drops below $\sim 2 \times 10^{-3}$ Pa^{-1}, whereas width decreases. The extent of bed cover drops with increasing rock strength to a minimum at intermediate to high strengths, depending on drainage area. For very hard rocks cover rises again. Then, the channel is still in the tools-dominated regime and the increase of cover corresponds to an increase in erosion rate, which is necessary to counteract the decrease in erosion rate due to the decrease in erodibility.

5. Discussion

5.1. Modeling the Cover Effect

[31] Fluvial erosion models without a cover term or with a linear cover formulation fail to fit experimental observations of wear at high sediment transport rates. The modified *Sklar and Dietrich* [2004] abrasion model combined with an exponential formulation for the cover effect provides a very good description of the experimental sediment load-erosion rate data obtained by *Sklar and Dietrich* [2001] for all sediment transport rates.

[32] Predicted erosion rates using equation (19) give realistic values for field settings. However, these values are sensitive to the input parameters. As an example, the long-term average channel-lowering rate at SFEC has been estimated at 0.9 mm a^{-1} from dated river terraces [*Merritts and Bull*, 1989]. By varying φ, d and τ_c, erosion rates predicted for this river range between about 0.1 and 2.5 mm a^{-1}. Using values listed in Table 1 gives results at the top end of this range. Furthermore, erosion rate is inversely proportional to the rock resistance coefficient k_v, for which only an order of magnitude estimate is available [*Sklar and Dietrich*, 2001, 2004] (Appendix A). Parameters characterizing rock strength can vary considerably in a series of tests on the same rock (e.g., tensile strength measurements commonly show deviations of more than 20% of the mean). Other values may vary spatially over short distances (e.g., substrate properties) or in time (e.g., median grain size).

[33] Erosion rates in the Liwu River have been measured in several ways. Direct measurements of erosion at Lushui station since 2000 have yielded an average rate of 5.5 mm a^{-1} [*Hartshorn et al.*, 2002; also unpublished data,

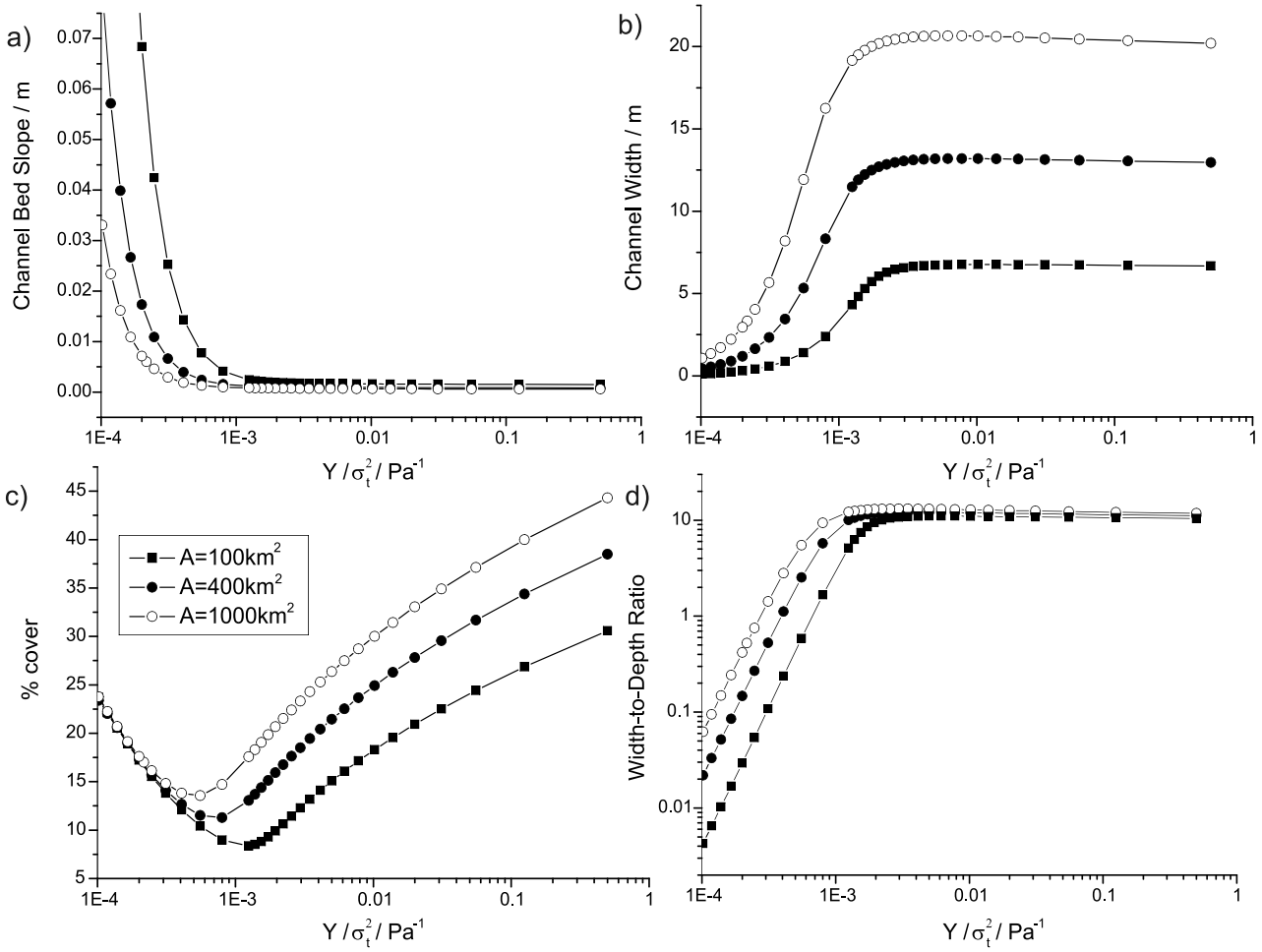

Figure 6. (a) Slope, (b) width, (c) bed cover, and (d) width-to-depth ratio as functions of the ratio of Young's modulus to the square of the rock tensile strength. Legend for all plots is shown in Figure 6c.

2001–2007]; the catchment-wide erosion rate over the past 30 a estimated from river gauging data is 12.5 mm a^{-1} [*Dadson et al.*, 2003]; dated strath terraces give millennial fluvial incision rates of 6 mm a^{-1} and 11 mm a^{-1} [*Liew*, 1988]; and average mid to late Holocene incision rates from cosmogenic nuclide analysis are 26 mm a^{-1} [*Schaller et al.*, 2005]. Incision rates predicted by our model range from 16 mm a^{-1} to 45 mm a^{-1}, at the top end of the measured rates. Predicted values are most likely to correspond to the catchment-wide erosion rates reported by *Dadson et al.* [2003], as we have used the same data set to estimate the erosive high flow discharge and associated sediment flux. It should be noted that predicted incision rates are likely to decrease when the history of sediment storage in the channel is taken into account. A large flood due to typhoon Long Wang in October 2005 left large amounts of sediment in the Liwu River, which took several months to evacuate. During this time bedrock erosion was minimal because of complete cover. Predicted wear rates are therefore likely to overestimate incision.

[34] The quality of the model predictions is affected by a large number of simplifications, notably the rectangular channel cross section, straight channels, $\varphi = 1$, effective discharge, and effective grain size; together with uncertainties on field measurements of long-term incision rate, rock strength, and grain size distribution. The cover factor φ, the rock resistance coefficient k_v, and the effective discharge are arguably the least well defined, with only weak, empirical constraints. Moreover, even when abrasion is the dominant mechanism of bedrock channel wear, other mechanisms such as quarrying, plucking, solution and cavitation can play an important role [*Hancock et al.*, 1998; *Hartshorn et al.*, 2002; *Snyder et al.*, 2003a; *Whipple et al.*, 2000; *Whipple*, 2004]. For example, at Lushui station, block removal is an important wear mechanism during floods, which are predominantly responsible for widening of the channel [*Hartshorn et al.*, 2002]. Although impacting particles may drive block removal, the abrasion equation does not provide an accurate description of this mechanism.

[35] Uncertainties in field and lab parameters and model simplifications make a useful comparison with other models for bedrock channel geometry difficult. Furthermore, the necessary data is available only for a few field sites. More, and more detailed field studies are needed to supply this data and to discriminate between available erosion laws.

5.2. Predicted Steady State Geometry

[36] Model predictions show some differences from models commonly applied to interpret natural data on channel

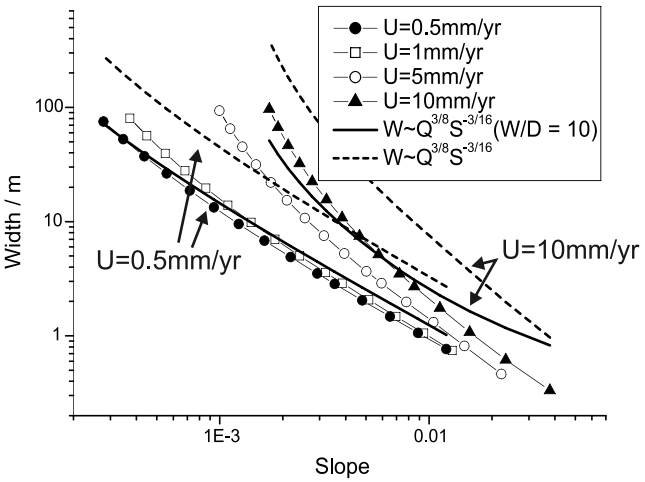

Figure 7. Predicted long-profile relationship between channel bed slope and width, for various uplift rates. The lines are comparisons with the *Finnegan et al.* [2005] model (equation (28)) at $U = 0.5$ mm a^{-1} (low values) and $U = 10$ mm a^{-1} (high values), using a constant width-to-depth ratio of 10 (solid lines) and the width-to-depth ratios predicted by our model (dashed lines; cf. Figure 3d).

geometry. For example, slope-area relationships are commonly modeled by power laws, giving a straight line in log-log space [e.g., *Hack*, 1957; *Flint*, 1974; *Tarboton et al.*, 1989; *Whipple*, 2004]. Concave-up slope-area relationships in log-log space, as in our model, have been predicted with various sediment-dependent incision models [*Whipple and Tucker*, 2002], using different formulations of the tools and cover effect, including a simplified version of the *Sklar and Dietrich* [1998] model. Models tested by *Whipple and Tucker* [2002] exhibit a strongly curved slope-area relationship in log-log space that is inconsistent with observations. Although the curvature predicted by our model is much smaller, we are not aware of any published field examples that clearly exhibit this mode of slope-area scaling. However, if the curved slope-area relation does exist in nature, then it is likely to be masked by large scatter in slope-area data, for example, because of DEM quality and/or spatial variability of rainfall, rock uplift rate, and substrate properties. Curvature of predicted slope-area scaling is likely to be reduced by inclusion of downstream-fining into the model [cf. *Whipple and Tucker*, 2002]. Regardless, forced power law fits to the slope-area data from our model have exponent values between about -0.35 and -0.50, depending on drainage area. This is within the range of values (-0.3 to -0.6) reported for natural bedrock rivers [*Whipple*, 2004].

[37] While width-discharge scaling relationships converge with the commonly used power law models with an exponent of $\sim$0.5 [*Leopold and Maddock*, 1953; *Park*, 1977], width-uplift relations are not well constrained in nature. Field studies report either a reduction in width with increasing uplift rate [*Duvall et al.*, 2004; *Harbor*, 1998; *Lavé and Avouac*, 2001; *Amos and Burbank*, 2007; *Whittaker et al.*, 2007], or no change at all [*Snyder et al.*, 2003a]. These observations are consistent with our model predictions: whereas channel response is in the threshold-limited domain in the case observed by *Snyder et al.* [2003a], it is dominated by uplift in the other studies.

[38] Assuming a constant width-to-depth ratio for a given channel type, *Finnegan et al.* [2005] have derived a scaling between width, discharge and slope, which is given by the equation

$$W = \left[\frac{W}{D}\left(\frac{W}{D}+2\right)^{2/3}\right]^{3/8} Q^{3/8} S^{-3/16} n^{3/8}. \quad (28)$$

In agreement with equation (28), *Wobus et al.* [2006b] have found a roughly constant width-to-depth ratio in their model of a detachment-limited channel with freely adjustable cross section. Moreover, in their model, width scales with slope according to a power law with an exponent of ~ -0.2. However, as pointed out by *Turowski et al.* [2006], hydraulic geometry data reported by *Leopold and Maddock* [1953] and subsequent workers show a weak power law scaling of the width-to-depth ratio with discharge with an exponent of around 0.1. In our model, the width-to-depth ratio is a function of drainage area (Figure 3d) with a weak scaling similar to the data of *Leopold and Maddock* [1953] (forced power law fits have exponents between $\sim$0.08 and $\sim$0.25 for the data shown in Figure 3d), uplift rate (Figure 4d) and erodibility (Figure 6d). We believe that the prediction of a roughly constant width-to-depth ratio in the *Wobus et al.* [2006b] model is an artifact of the lack of a critical shear stress for the onset of erosion, and the absence of sediment transport and its effects on bedrock incision from the model.

[39] Figure 7 shows the scaling between width and slope for various uplift rates. Relationships are slightly concave up in log-log space, with a more pronounced curvature for higher uplift rates. Solid lines are predictions using equation (27) with a constant width-to-depth ratio of ten. Dashed lines were obtained with the same equation, using width-to-depth ratios corresponding to width and slope values as predicted by our model (cf. Figure 3). Although the latter approach traces functional forms better than the former, absolute width values differ from model results by a factor of about five.

[40] *Whittaker et al.* [2007] have found a relatively low scaling exponent of ~ -0.34 for width and slope data from channels crossing the Fiamignano fault in the Italian Appenines. They have concluded that these channels are in a transient state, responding to an increase in uplift rate about 1 million a ago, and suggested that stronger nonlinear scaling may be a signature of transient channels. However, a similar effect is predicted by our model for steady state channels at higher uplift rates. The scaling exponent in the width-slope relation cannot be used to distinguish between transient or steady channel states.

[41] The predicted, progressive alluviation of bedrock channels with increasing drainage area is broadly consistent with field observations, but it is not associated with a very strong signal in the slope-area relationship. Correspondingly, we anticipate that it may be difficult to find a discernible geometric signature of tool-dominated regimes compared to cover-dominated regimes. This problem is increased by the large variability in extent and thickness of alluvial cover in mountain channels, caused by stochastic sediment supply

from hillslopes, modulated by the temporal variation in water discharge. Therefore it is hard to make a direct comparison between the short-term bed cover state, and slope-area relationships that are derived from models with longer timescales.

[42] To avoid the complexities arising from the combination of a complete water discharge distribution with an already complex incision model, and the minimization of potential energy, we have used an effective discharge of constant value, as did *Sklar and Dietrich* [2006]. Previous work has shown that at steady state, the effective discharge varies with uplift rate [*Snyder et al.*, 2003b; *Lague et al.*, 2005b]. Even though these previous studies did not allow for a width change with uplift rate or lithology, we expect that the scaling of slope with uplift rate at low uplift rates would be altered. For example, *Lague et al.* [2005b] have shown that the constant slope regime is replaced by a power law dependency between slope and uplift rate. Further work using both a full discharge distribution and freely variable width is needed.

6. Conclusion

[43] Using a probabilistic argument, we have derived an exponential formulation for the cover effect in bedrock river channels. This formulation can replace linear sediment load-cover relations in existing models of fluvial erosion such as the model of bedrock abrasion by saltating bed load by *Sklar and Dietrich* [2004], to obtain a very good match with experimental bedrock erosion rates for a wide range of sediment transport rates.

[44] In a closed system, our erosion model predicts that erosion rates do not vanish above certain values of grain size or transport stage, as in earlier studies, but rather approach zero asymptotically at infinity, giving small, but finite erosion rates for high ratios of sediment supply to transport capacity. In comparison with a linear model for the cover effect the new model predicts higher erosion rates. Differences between predictions increase with increasing ratio of sediment supply and transport capacity. Moreover, the maximum erosion rate predicted by our model is $\sim$1/3 larger, occurring when the sediment flux is equal to the transport capacity (assuming $\varphi = 1$), rather than at half the transport capacity, as with the linear formulation [*Sklar and Dietrich*, 1998, 2004].

[45] Parameterized in accordance with field and experimental observations, our model predicts river incision rates of the correct order of magnitude in well-documented settings. However, given the large number of parameters in the model, it is always possible to find a combination of values that will predict an observed incision rate. Therefore we view this work as a further step toward better understanding of the relationship between incision, sediment flux and channel geometry in bedrock rivers, rather than as an operational tool for precise calculation of long-term bedrock incision rates for given boundary conditions.

[46] Assuming minimization of potential energy expenditure, we have used the described erosion model to derive relationships between channel morphology (slope, width, bed cover, width-to-depth ratio) and boundary conditions (discharge, erosion rate, sediment supply). We predict a slightly concave-up slope-area relationship in log-log space whose degree of curvature is a function of rock uplift rate. This deviation from the received, power law behavior of a simple, detachment-limited model arises from the progressive downstream increase of alluvial cover, and a shift from a tools-dominated regime for small drainage areas/discharges to a cover-dominated regime for large drainage areas/discharges. For realistic values of drainage area and uplift rate, available data do not allow clear discrimination between the model derived herein and a straight power law relationship between channel bed slope and drainage area.

[47] The variation of channel slope with uplift rate tracks results from a simple shear stress model [*Lague et al.*, 2005a]. This is not the case for channel width, which we predict to increase with uplift rate, and then to decrease more rapidly than in the simple shear stress model. For small values of uplift rate both width and slope are largely insensitive to variations in tectonic forcing. This is due to a threshold effect. The lack of detailed field data, and the use of a constant effective discharge instead of the full water and sediment discharge distribution, currently limit the applicability of this particular result. However, the result highlights how scaling of channel width and rock uplift rate could be used as an additional constraint for the characterization and validation of incision laws.

[48] The channel width-to-depth ratio is predicted to vary with both drainage area and uplift rate. This indicates that the scaling between channel width and bed slope is neither a unique indicator of tectonic forcing at steady state, as suggested by *Finnegan et al.* [2005], nor a signature of transience or steady state, as suggested by *Whittaker et al.* [2007].

[49] Because of threshold effects, channel geometry is found to be insensitive to varying rock strength for weak to intermediate strength substrates. In such substrates, erosion rates are adjusted instead by variation of the alluvial cover. As rock strength increases, channel slope and width adjust to increase shear stress and cover drops to a minimum, before it rises again to counteract the rapid increase in slope.

[50] Further experimental work and tighter constraints on rates and characteristics of representative bedrock rivers, especially direct observations of bed cover over a range of conditions, should help test and refine the proposed alluvial cover model and more generally the *Sklar and Dietrich* [2004] abrasion model, enabling their use in evaluations of the long-term incision of mountain channels.

Appendix A: Estimation of the Rock Resistance Coefficient k_v

[51] The ratio of the sediment mass to the sediment mass transport capacity m_s/m_t is equal to the ratio of sediment flux to sediment transport capacity (see section 2.2.2):

$$\frac{m_s}{m_t} = \frac{q_s}{q_t}. \tag{A1}$$

The normalized erosion rate can then be written as

$$E' = E\sigma_t^2\rho_s a_{tot} = KS_e\sigma_t^2\rho_s a_{tot} q_s e^{-\varphi\frac{q_s}{q_t}} = K' m_s e^{-\varphi\frac{m_s}{m_t}} \tag{A2}$$

with

$$KS_e\sigma_t^2\rho_s a_{tot} q_s = KS_e\sigma_t^2\rho_s a_{tot} q_t \frac{m_s}{m_t} = K' m_s. \quad \text{(A3)}$$

By using the equation

$$E' = K' m_s e^{-\varphi\frac{m_s}{m_t}} \quad \text{(A4)}$$

to fit to the data in Figure 1, m_t/φ and K' can be found. At the maximum $m_s = m_t/\varphi$, as well as $q_s = q_t/\varphi$. An order of magnitude estimate for the sediment flux and hence the transport capacity at the maximum erosion rate can be obtained from data given by *Sklar and Dietrich* [2001]. The sediment flux is given by

$$q_s = \frac{VA_c}{W}\rho_s = \frac{\omega l}{2}\frac{lh}{l}\rho_s. \quad \text{(A5)}$$

Here $l = 11$ cm is the radius of the tank, $h \sim 2$–3 cm the maximum height of transport above the bed, and $\omega = 1000$ rpm the angular velocity. The factor of 1/2 is introduced to obtain the velocity at half radius. Considering that the angular velocity is given some distance above the bed and that the sediment will probably move slower than the water, a transport capacity of $q_t/\varphi \sim 20$ kg m^{-1} s^{-1} seems reasonable.

[52] Assuming that the transport capacity does not change with changing sediment mass, the transport stage can be estimated using the bed load transport equation (13):

$$T_s = \frac{\tau^*}{\tau_c^*} = 1 + \left(\frac{q_t}{5.7\rho_s}\right)^{2/3}\left(\frac{\rho_w}{\Delta\rho g}\right)^{1/3}\frac{1}{\tau_c^* d}. \quad \text{(A6)}$$

Using a value of 0.03 for the critical shear stress for the onset of motion from Yalin's curve for a grain size of 6 mm gives $T_s = 27.5$, so the suspension effect term (equation (3)) cannot be neglected. The particle fall velocity has been calculated using the method of *Dietrich* [1982]. The rock resistance coefficient k_v can then be written as

$$k_v = \frac{0.08\Delta\rho g Y \rho_s a_{tot} q_t S_e}{K'\rho_w m_t}(T_s - 1)^{-1/2}. \quad \text{(A7)}$$

Given that $K' = (0.50 \pm 0.02)$ MPa^2 h^{-1} and $m_t/\varphi = (133.7 \pm 4.2) \times 10^{-3}$ kg from a nonlinear fit to the data in Figure 1 and $a_{tot} = 1.2 \times \pi \times 10^{-2}$ m^2 [*Sklar and Dietrich*, 2001], $k_v \sim 10^6$.

Appendix B: Constitutive Equations and Derivation

[53] The channel geometry is controlled by the three independent parameters erosion rate E, water discharge Q, and sediment supply Q_s; and is specified by the geometric channel bed slope S, parameters width W, depth D, cross-sectional area A_c, wetted perimeter P_w, and hydraulic radius R_h, and the hydraulic parameters flow velocity V and bed shear stress τ_b. The median grain size is assumed to be independent of drainage area, as argued by *Attal and Lavé* [2006]. The eight dependent parameters are related by four general equations:

$$\text{the continuity equation} \quad Q = VA_c \quad \text{(B1)}$$

$$\text{the force balance at the bed} \quad \tau_b = \rho_w R_h S \quad \text{(B2)}$$

$$\text{the Manning flow resistance equation} \quad V = \frac{1}{n}R_h^{2/3}S^{1/2} \quad \text{(B3)}$$

$$\text{the definition of the hydraulic radius} \quad R_h = \frac{A_c}{P_w}. \quad \text{(B4)}$$

An additional two equations come from the assumption of a rectangular cross section:

$$\text{the cross–sectional area} \quad A_c = WD \quad \text{(B5)}$$

$$\text{and the wetted perimeter} \quad P_w = 2D + W. \quad \text{(B6)}$$

To close the system, two additional equations are necessary. We use the erosion law derived above (equation (13)):

$$E = \frac{CQ_s}{W}\left(\frac{\tau_b}{\tau_c} - 1\right)^{-1/2}\exp\left(-\frac{BQ_s}{W}\left(\frac{\tau_b}{\tau_c} - 1\right)^{-3/2}\right), \quad \text{(B7)}$$

with

$$B = \frac{\varphi\Delta\rho g}{5.7\rho_s}\left(\frac{\rho_w}{\tau_c^3}\right)^{1/2} \quad \text{(B8)}$$

and

$$C = \frac{0.08\Delta\rho g Y}{k_v\rho_w\sigma_t^2}, \quad \text{(B9)}$$

and the optimization of potential energy expenditure [*Lague et al.*, 2005a]

$$\frac{dS}{dW} = 0. \quad \text{(B10)}$$

Using equations (B1)–(B6) to eliminate all parameters apart from S, W, and τ_b gives:

$$2nQ\frac{\tau_b}{\rho_w g} = nQSW - W^2 S^{-1/6}\left(\frac{\tau_b}{\rho_w g}\right)^{5/3}. \quad \text{(B11)}$$

Taking the derivative with respect to W, applying (B10), rewriting with the help of (B11), and solving for S:

$$S = \frac{\tau_b}{\rho_w g}\frac{2}{W}\frac{2 + \frac{2}{3}\frac{W}{\tau_b}\frac{d\tau_b}{dW}}{1 + \frac{5}{3}\frac{W}{\tau_b}\frac{d\tau_b}{dW}}. \quad \text{(B12)}$$

(B12) can be used to eliminate S in (B11):

$$2^{5/6}\left(1-\frac{W}{\tau_b}\frac{d\tau_b}{dW}\right)nQ = W^{11/6}\left(2+\frac{2}{3}\frac{W}{\tau_b}\frac{d\tau_b}{dW}\right)^{-1/6} \cdot \left(1+\frac{5}{3}\frac{W}{\tau_b}\frac{d\tau_b}{dW}\right)^{5/6}\left(\frac{\tau_b}{\rho_w g}\right)^{1/2}. \quad \text{(B13)}$$

To eliminate $\frac{d\tau_b}{dW}$, take the derivative of (B7) and solve:

$$\frac{d\tau_b}{dW} = -\frac{2\tau_c}{W}\left(\frac{\tau_b}{\tau_c}-1\right)\frac{BQ_s - W\left(\frac{\tau_b}{\tau_c}-1\right)^{3/2}}{3BQ_s - W\left(\frac{\tau_b}{\tau_c}-1\right)^{3/2}}. \quad \text{(B14)}$$

Substituting (B14) into (B12) gives an equation of the form $S = f(W, \tau_b, Q_s)$. To arrive at a solution it is necessary to make the substitution

$$\Phi = W^{-1}\left(\frac{\tau_b}{\tau_c}-1\right)^{-3/2}. \quad \text{(B15)}$$

The erosion law (B7) can then be written as

$$\left(\frac{\tau_b}{\tau_c}-1\right) = \frac{E}{CQ_s\Phi}\exp(BQ_s\Phi). \quad \text{(B16)}$$

Substituting equations (B14)–(B16) into equation (B13), one obtains

$$2^{4/3}\left(1+\frac{2E\exp(BQ_s\Phi)}{(E\exp(BQ_s\Phi)+CQ_s\Phi)}\frac{BQ_s\Phi-1}{3BQ_s\Phi-1}\right) \cdot \left(\frac{CQ_s\Phi\rho_w g}{E\exp(BQ_s\Phi)+CQ_s\Phi}\right)^{1/2} nQ = \Phi^{13/12}\left(\frac{E}{CQ_s}\exp(BQ_s\Phi)\right)^{-13/4} \cdot \left(1-\frac{2E\exp(BQ_s\Phi)}{3(E\exp(BQ_s\Phi)+CQ_s\Phi)}\frac{BQ_s\Phi-1}{3BQ_s\Phi-1}\right)^{-1/6} \cdot \left(1-\frac{10E\exp(BQ_s\Phi)}{3(E\exp(BQ_s\Phi)+CQ_s\Phi)}\frac{BQ_s\Phi-1}{3BQ_s\Phi-1}\right)^{7/6}. \quad \text{(B17)}$$

This equation allows the calculation of Φ as a function of the boundary condition E, Q_s and Q (factors like rock strength or critical shear stress are encompassed in the parameters B and C). For given Φ, τ_b can be calculated from equation (B16). W is then computed from equation (B15), and slope S using equations (B12) and (B14).

[54] Equation (B17) has generally only one physically possible solution (real positive slope and width). However, in some cases it generates two or more configurations, that correspond to local minima of the $S = f(W)$ relationship (i.e., $dS/dW = 0$). However, these solutions can be neglected, as they predict clearly unrealistic values for width, slope and flow velocity (several orders of magnitude too high or too low) and show incorrect scaling behavior with drainage area.

Notation

A upstream drainage area, m^2.
a_{exp} exposed bed area, m^2.
a_{tot} total bed area, m^2.
B constant prefactor in exponent, m kg^{-1} s.
C constant prefactor of erosion law, m^{-2}.
D flow depth, m.
d representative grain size, m
E erosion rate, m s^{-1}.
E' normalized erosion rate, Pa^2 kg s^{-1}.
F net transfer from suspended load to bed load, m s^{-1}.
e base of the natural logarithm.
g acceleration due to gravity, m s^{-2}.
h thickness of sediment stored in the channel, m.
I_r particle impact rate, m^{-2} s^{-1}.
k_e prefactor simple shear stress incision law, m kg^{-1}.
K erosion factor (flux), m^{-2} kg^{-1}.
K' normalized erosion constant (mass), Pa^2 s^{-1}.
K_m erosion factor (mass), m^{-2} kg^{-1} s^{-1}.
k_v dimensionless rock resistance coefficient.
l radius of experimental tank, m.
m_i sediment mass stored in the channel, kg.
m_s sediment mass supplied from upstream, kg.
m_t sediment mass transport capacity, kg.
n Manning's roughness coefficient, $m^{-1/3}$ s.
P average precipitation rate, m s^{-1}.
q_s sediment supply per unit width, kg m^{-1} s^{-1}.
q_f sediment flux per unit width, kg m^{-1} s^{-1}.
q_t transport capacity per unit width, kg m^{-1} s^{-1}.
Q water discharge, m^3 s^{-1}.
Q_s sediment supply, kg/s.
R_a fraction of exposed bed area.
R_h hydraulic radius, m.
S channel bed slope.
S_e suspension effect term.
t time, s.
T_s transport stage.
U uplift rate, m s^{-1}.
u^* shear velocity, m s^{-1}.
V flow velocity averaged over channel cross section, m s^{-1}.
W flow width, m.
w_f particle settling velocity, m s^{-1}.
x along-stream distance, m.
Y Young's modulus of substrate, Pa.
β fraction of sediment transported as bed load.
κ dimensionless constant of integration.
$\Delta\rho$ density difference between sediment and water, kg m^{-3}.
ρ_s density of sediment, kg m^{-3}.
ρ_w density of water, kg m^{-3}.
σ_t rock tensile strength, Pa.
τ^* Shields stress.
τ_c^* critical Shields stress.
τ_b bed shear stress, Pa.
τ_c critical shear stress, Pa.
φ cover factor.
Φ variable dependent on shear stress and width, m^{-1}.
ω angular velocity, s^{-1}.

[55] **Acknowledgments.** Thanks to R. Hilton for critical reading of an early version of the manuscript. Discussions with L. Sklar and J. Lavé are gratefully acknowledged. Constructive reviews by A. L. Densmore, A. D. Howard, and P. Bishop have helped to improve the work considerably. J. M. T. was supported by a Blue Skies Studentship from NERC. Additional funds came from the Cambridge Trusts and CNRS-INSU program RELIEFS.

References

Amos, C. B., and D. W. Burbank (2007), Channel width response to differential uplift, *J. Geophys. Res.*, *112*, F02010, doi:10.1029/2006JF000672.

Attal, M., and J. Lavé, (2006), Changes of bedload characteristics along the Marsyandi River (central Nepal): Implications for understanding hillslope sediment supply, sediment load evolution along fluvial networks and denudation in active orogenic belts, in *Tectonics, Climate and Landscape Evolution*, edited by S. D. Willett et al., *Geol. Soc. Am. Spec. Publ.*, *398*, 143–171.

Attal, M., J. Lavé, and J. P. Masson (2006), New facility to study river abrasion processes, *J. Hydraul. Eng.*, *132*, 624–628.

Dadson, S. J., et al. (2003), Links between erosion, runoff variability and seismicity in the Taiwan orogen, *Nature*, *426*, 648–651.

Dietrich, W. E. (1982), Settling velocity of natural particles, *Water Resour. Res.*, *18*, 1615–1626.

Duvall, A., E. Kirby, and D. Burbank (2004), Tectonic and lithologic controls on bedrock channel profiles and processes in coastal California, *J. Geophys. Res.*, *109*, F03002, doi:10.1029/2003JF000086.

Eaton, B. C., M. Church, and R. G. Millar (2004), Rational regime model of alluvial channel morphology and response, *Earth Surf. Processes Landforms.*, *29*, 511–529.

Fernandez Luque, R., and R. van Beek (1976), Erosion and transport of bed-load sediment, *J. Hydraul. Res.*, *14*, 127–144.

Finnegan, N. J., G. Roe, D. R. Montgomery, and B. Hallet (2005), Controls on the channel width of rivers: Implications for modelling fluvial incision of bedrock, *Geology*, *33*(3), 229–232, doi:10.1130/G21171.1.

Finnegan, N. J., L. S. Sklar, and T. K. Fuller (2007), Interplay of sediment supply, river incision, and channel morphology revealed by the transient evolution of an experimental bedrock channel, *J. Geophys. Res.*, 112, F03S11, doi:10.1029/2006JF000569.

Flint, J.-J. (1974), Stream gradient as a function of order, magnitude and discharge, *Water Resour. Res.*, *10*, 969–973.

Foley, M. G. (1980), Bed-rock incision by streams, *Geol. Soc. Am. Bull.*, *91*, 2189–2213.

Gilbert, G. K. (1877), Land sculpture, in *The Geology of the Henry Mountains, Utah*, edited by C. B. Hunt, chap. 5, *Mem. Geol. Soc. Am.*, *167*, 99–150.

Hack, J. T. (1957), Studies of longitudinal stream profiles in Virginia and Maryland, *U. S. Geol. Surv. Prof. Pap.*, *294*, 45–80.

Hancock, G., and R. S. Anderson (2002), Numerical modeling of fluvial strath terrace formation in response to oscillating climate, *Geol. Soc. Am. Bull.*, *114*, 1131–1142.

Hancock, G., R. S. Anderson, and K. X. Whipple (1998), Beyond power: Bedrock river incision process and form, in *Rivers Over Rock: Fluvial Processes in Bedrock Channels*, edited by K. J. Tinkler and E. E. Wohl, *Geophys. Monogr. Ser.*, vol. 107, pp. 35–60, AGU, Washington, D. C.

Harbor, D. J. (1998), Dynamic equilibrium between an active uplift and the Sevier River, Utah, *J. Geol.*, *106*, 181–194.

Hartshorn, K., N. Hovius, W. B. Dade, and R. L. Slingerland (2002), Climate-driven bedrock incision in an active mountain belt, *Science*, *297*, 2036–2038.

Howard, A. D. (1994), A detachment-limited model of drainage basin evolution, *Water Resour. Res.*, *30*, 2261–2285.

Howard, A. D., and G. Kerby (1983), Channel changes in badlands, *Geol. Soc. Am. Bull.*, *94*, 739–752.

Huang, H. Q., and G. C. Nanson (2002), A stability criterion inherent in laws governing alluvial channel flow, *Earth Surf. Processes Landforms*, *27*, 929–944.

Huang, H. Q., H. H. Chang, and G. C. Nanson (2004), Minimum energy as the general form of critical flow and maximum flow efficiency and for explaining variations in river channel pattern, *Water Resour. Res.*, *40*, W04502, doi:10.1029/2003WR002539.

Kooi, H., and C. Beaumont (1996), Large-scale geomorphology: Classical concepts reconciled and integrated with contemporary ideas via a surface processes model, *J. Geophys. Res.*, *101*, 3361–3386.

Lague, D., J. M. Turowski, P. Davy, and N. Hovius (2005a), The width (and slope) of an incising river: Analytical solution and comparison with natural and experimental rivers, paper presented at General Assembly 2005, Eur. Geosci. Union, Vienna.

Lague, D., N. Hovius, and P. Davy (2005b), Discharge, discharge variability, and the bedrock channel profile, *J. Geophys. Res.*, *110*, F04006, doi:10.1029/2004JF000259.

Lavé, J., and J. P. Avouac (2001), Fluvial incision and tectonic uplift across the Himalayas of central Nepal, *J. Geophys. Res.*, *106*, 26,561–26,592.

Leopold, L. B., and T. Maddock Jr. (1953), The hydraulic geometry of stream channels and some physiographic implications, *U.S. Geol. Surv. Prof.*, *252*.

Liew, P. M. (1988), Sedimentology and river-terrace correlation of the Liwu River (in Chinese), technical report, Natl. Taiwan Univ., Taipei, Taiwan.

Manning, R. (1891), On the flow of water in open channels and pipes, *Trans. Inst. Civ. Eng.*, *20*, 161–207.

Merritts, D. J., and W. B. Bull (1989), Interpreting Quaternary uplift rates at the Mendocino triple junction, northern California, from uplifted marine terraces, *Geology*, *17*, 1020–1024.

Moore, R. C. (1926), Origin of enclosed meanders on streams of the Colorado plateau, *J. Geol.*, *34*, 29–57.

Paola, C., and V. R. Voller (2005), A generalized Exner equation for sediment mass balance, *J. Geophys. Res.*, *110*, F04014, doi:10.1029/2004JF000274.

Park, C. C. (1977), World-wide comparison in hydraulic geometry exponents of stream channels: An analysis and some observation, *J. Hydrol.*, *33*, 133–146.

Schaller, M., N. Hovius, S. D. Willett, S. Ivy-Ochs, H.-A. Synal, and M.-C. Chen (2005), Fluvial bedrock incision in the active mountain belt of Taiwan from in-situ produced cosmogenic nuclides, *Earth Surf. Processes Landforms*, *30*, 955–971.

Shepherd, R. C. (1972), Incised river meanders: Evolution in simulated bedrock, *Science*, *178*, 409–411.

Sklar, L., and W. E. Dietrich (1998), River longitudinal profiles and bedrock incision models: Stream power and the influence of sediment supply, *Rivers Over Rock: Fluvial Processes in Bedrock Channels*, edited by K. J. Tinkler and E. E. Wohl, *Geophys. Monogr. Ser.*, vol. 107, pp. 237–260, AGU, Washington, D. C.

Sklar, L., and W. E. Dietrich (2001), Sediment and rock strength controls on river incision into bedrock, *Geology*, *29*, 1087–1090, doi:10.1130/0091-7613(2001)029<1087:SARSCO>2.0.CO;2.

Sklar, L. S., and W. E. Dietrich (2004), A mechanistic model for river incision into bedrock by saltating bed load, *Water Resour. Res.*, *40*, W06301, doi:10.1029/2003WR002496.

Sklar, L., and W. E. Dietrich (2006), The role of sediment in controlling steady-state bedrock channel slope: Implications of the saltation-abrasion incision model, *Geomorphology*, *82*, 58–83, doi:10.1016/j.geomorph.2005.08.019.

Slingerland, R., S. D. Willett, and H. L. Hennessey (1997), A new fluvial bedrock incision model based on the work-energy principle, *Eos Trans. AGU*, *78*(46), Fall Meet. Suppl., Abstract H42F-12.

Snyder, N. P., K. X. Whipple, G. E. Tucker, and D. J. Merritts (2003a), Channel response to tectonic forcing: Field analysis of stream morphology and hydrology in the Mendocino triple junction region, northern California, *Geomorphology*, *53*, 97–127, doi:10.1016/S0169-555X(02)00349-5.

Snyder, N. P., K. X. Whipple, G. E. Tucker, and D. J. Merritts (2003b), Importance of a stochastic distribution of floods and erosion thresholds in the bedrock river incision problem, *J. Geophys. Res.*, *108*(B2), 2117, doi:10.1029/2001JB001655.

Stark, C. P. (2006), A self-regulating model of bedrock river channel geometry, *Geophys. Res. Lett.*, *33*, L04402, doi:10.1029/2005GL023193.

Talling, P. J. (2000), Self-organization of river networks to threshold states, *Water Resour. Res.*, *36*, 1119–1128.

Tarboton, D. G., R. L. Bras, and I. Rodriguez-Iturbe (1989), Scaling and elevation in river networks, *Water Resour. Res.*, *25*, 2037–2051.

Turowski, J. M., D. Lague, A. Crave, and N. Hovius (2006), Experimental channel response to tectonic uplift, *J. Geophys. Res.*, *111*, F03008, doi:10.1029/2005JF000306.

Turowski, J. M., N. Hovius, Hsieh Meng-Long, D. Lague, and Chen Men-Chiang (2007), Distribution of erosion across bedrock channels, *Earth Surf. Processes Landforms*, in press.

Whipple, K. X. (2004), Bedrock rivers and the geomorphology of active orogens, *Annu. Rev. Earth Planet. Sci.*, *32*, 151–185, doi:10.1146/annurev.earth.32.101802.120356.

Whipple, K. X., and G. E. Tucker (1999), Dynamics of the stream-power river incision model: Implications for height limits of mountain ranges, landscape response timescales, and research needs, *J. Geophys. Res.*, *104*, 17,661–17,674.

Whipple, K. X., and G. E. Tucker (2002), Implications of sediment-flux-dependent river incision models for landscape evolution, *J. Geophys. Res.*, *107*(B2), 2039, doi:10.1029/2000JB000044.

Whipple, K. X., G. S. Hancock, and R. S. Anderson (2000), River incision into bedrock: Mechanics and relative efficacy of plucking, abrasion, and cavitation, *Geol. Soc. Am. Bull.*, *112*, 490–503, doi:10.1130/0016-7606(2000)112<0490:RIIBMA>2.3.CO;2.

Whittaker, A. C., P. A. Cowie, M. Attal, G. E. Tucker, and G. P. Roberts (2007), Bedrock channel adjustment to tectonic forcing: Implications for predicting river incision rates, *Geology*, *35*, 103–106, doi:10.1130/G23106A.1.

Wobus, C. W., B. T. Crosby, and K. X. Whipple (2006a), Hanging valleys in fluvial systems: Controls on occurrence and implications for landscape evolution, *J. Geophys. Res.*, *111*, F02017, doi:10.1029/2005JF000406.

Wobus, C. W., G. E. Tucker, and R. S. Anderson (2006b), Self-formed bedrock channels, *Geophys. Res. Lett.*, *33*, L18408, doi:10.1029/2006GL027182.

Wohl, E. E., and H. Ikeda (1997), Experimental simulation of channel incision into a cohesive substrate at varying gradients, *Geology*, *25*, 295–298, doi:10.1130/0091-7613(1997)025<0295:ESOCII>2.3.CO;2.

N. Hovius, Department of Earth Sciences, University of Cambridge, Downing Street, Cambridge CB2 3EQ, UK.

D. Lague, UMR 6118, Géociences Rennes, Université Rennes I, INSU, CNRS, Campus de Beaulieu, F-35042 Rennes cedex, France.

J. M. Turowski, Swiss Federal Institute for Forest, Snow and Landscape Research, CH-8903 Birmensdorf, Switzerland. (jens.turowski@wsl.ch)